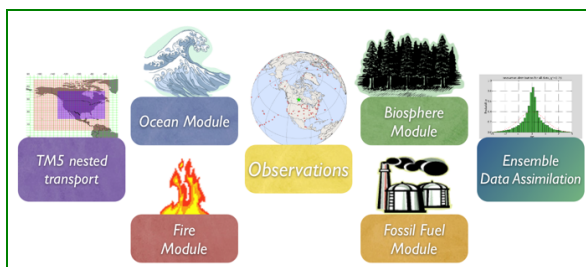


Documentation – CTE2015



To learn more about a CarbonTracker component, click on one of the above images.
Or [download the full PDF version](#) for convenience.

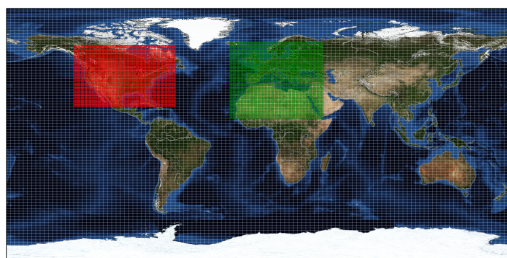
TMS Nested Transport [\[go to top\]](#)

1. Introduction

The link between observations of CO₂ in the atmosphere and the exchange of CO₂ at the Earth's surface is transport in the atmosphere: storm systems, cloud complexes, and weather of all sorts cause winds that transport CO₂ around the world. As a result, local events like fires, forest growth, and ocean upwelling can have impacts at remote locations. To simulate the winds and the weather, CarbonTracker uses sophisticated numerical models that are driven by the daily weather forecasts from the specialized meteorological centers of the world. Since CO₂ does not decay or react in the lower atmosphere, the influence of emissions and uptake in locations such as North America and Europe are ultimately seen in our measurements even at the South Pole! Getting the transport of CO₂ just right is an enormous challenge, and costs us almost 90% of the computer resources for CarbonTracker. To represent the atmospheric transport, we use the Transport Model 5 (TMS). This is a community-supported model whose development is shared among many scientific groups with different areas of expertise. TMS is used for many applications other than CarbonTracker, including forecasting air-quality, studying the dispersion of aerosols in the tropics, tracking biomass burning plumes, and predicting pollution levels that future generations might have to deal with.

2. Detailed Description

TMS is a global model with two-way nested grids; regions for which high-resolution simulations are desired can be nested in a coarser grid spanning the global domain. The advantage to this approach is that transport simulations can be performed with a regional focus without the need for boundary conditions from other models. Further, this approach allows measurements outside the "zoom" domain to constrain regional fluxes in the data assimilation, and ensures that regional estimates are consistent with global constraints. TMS is based on the predecessor model TM3, with improvements in the advection scheme, vertical diffusion parameterization, and meteorological preprocessing of the wind fields (Krol et al., 2005). The model is developed and maintained jointly by the [Institute for Marine and Atmospheric Research Utrecht \(IMAU, The Netherlands\)](#), the [Joint Research Centre \(JRC, Italy\)](#), the [Royal Netherlands Meteorological Institute \(KNMI, The Netherlands\)](#), and [NOAA ESRL \(USA\)](#). In CarbonTracker, TMS separately simulates advection, convection (deep and shallow), and vertical diffusion in the planetary boundary layer and free troposphere.



The winds which drive TMS come from the [European Center for Medium range Weather Forecast \(ECMWF\)](#) operational forecast model. This "parent" model currently runs with ~25 km horizontal resolution and 25 layers in the vertical. The carbon dioxide levels predicted by CarbonTracker do not feed back onto these predictions of winds. In contrast to earlier versions of CarbonTracker, we currently use the convection fields directly from ECMWF (whereas before they were calculated using the Tiedtke convection scheme).

For use in TMS, the ECMWF meteorological data are preprocessed into coarser grids. In CarbonTracker Europe, TMS is run at a global 3x2 degrees resolution with nested regions over Europe (1x1 degrees) and North America (1x1 degree). The grid over Europe is shown in the figure. TMS runs at an external time step of three hours, but due to the symmetrical operator splitting and the refined resolution in nested grids, processes at the finest scale are repeated every 10 minutes. The vertical resolution of TMS in CarbonTracker Europe is 25 hybrid sigma-pressure levels, unevenly spaced with more levels near the surface. Approximate heights of the mid-levels (in meters, with a surface pressure of 1012 hPa) are:

Level	Height (m)	Level	Height (m)
1	34.5	14	9076.6
2	111.9	15	10533.3
3	256.9	16	12108.3
4	490.4	17	13874.2
5	826.4	18	15860.1
6	1274.1	19	18093.2
7	1839.0	20	20590.0
8	2524.0	21	24247.3
9	3329.9	22	29859.6
10	4255.6	23	35695.0
11	5298.5	24	42551.5
12	6453.8	25	80000.0
13	7715.4		

3. Further Reading

- [The TMS model homepage](#)
- [ECMWF forecast model technical documentation](#)
- [Peters et al., 2004, JGR paper on transport in TMS](#)
- [Krol et al., 2005, ACP overview paper of the TMS model](#)

Oceans Module [\[go to top\]](#)

1. Introduction

The oceans play an important role in the Earth's carbon cycle. They are the largest long-term sink for carbon and have an enormous capacity to store and redistribute CO₂ within the system. Oceanographers estimate that about 48% of the CO₂ from fossil fuel burning has been absorbed by the ocean [Sabine et al., 2004]. The dissolution of CO₂ in seawater shifts the balance of the ocean carbonate equilibrium towards a more acidic state (i.e., with a lower pH). This effect is already measurable [Caldeira and Wickett, 2003], and is expected to become an acute challenge to shell-forming organisms over the coming decades and centuries. Although the oceans as a whole have been a relatively steady net carbon sink, CO₂ can also come out of the oceans depending on local temperatures, biological activity, wind speeds, and ocean circulation. These processes are all considered in CarbonTracker, since they can have significant effects on the ocean sink. Improved estimates of the air-sea exchange of carbon in turn help us to understand variability of both the atmospheric burden of CO₂ and terrestrial carbon exchange.

2. Detailed Description

Oceanic uptake of CO₂ in CarbonTracker is computed using air-sea differences in partial pressure of CO₂ inferred from ocean inversions, combined with a gas transfer velocity computed from wind speeds in the atmospheric transport model.

The long-term mean air-sea fluxes, and the uncertainties associated with them, derive from the ocean interior inversions reported in Jacobson et al. [2007]. These ocean inversion flux (OIF) estimates are composed of separate preindustrial (natural) and anthropogenic flux inversions based on the methods described in Gloor et al. [2003] and biogeochemical interpretations of Gruber, Sarmiento, and Stocker [1996]. The uptake of anthropogenic CO₂ by the ocean is assumed to increase in proportion to atmospheric CO₂ levels, consistent with estimates from ocean carbon models.

For CarbonTracker Europe, contemporary pCO₂ fields were computed by summing the preindustrial and anthropogenic flux components from inversions using five different configurations of the Princeton/GFDL MOM3 ocean general circulation model [Pacanowski and Gnanadesikan, 1998], then dividing by a gas transfer velocity computed from the European Centre for Medium-Range Weather Forecasts (ECMWF) ERA40 reanalysis. There are two small differences in first-guess fluxes in this computation from those reported in Jacobson et al. [2007]. First, the five OIF estimates all used Takahashi et al. [2002] pCO₂ estimates to provide high-resolution patterning of flux within inversion regions (the alternative "forward" model patterns were not used). To good approximation, this choice only affects the spatial and temporal distribution of flux within each of the **30 ocean inversion regions**, not the magnitude of the estimated flux. Second, wind speed differences between the ERA40 product used in the offline analysis and the ECMWF operational model used in the online CarbonTracker analysis result in small deviations from the OIF estimates.

Gas transfer velocity in CarbonTracker is parameterized as a quadratic function of wind speed following Wanninkhof [1992], using the formulation for instantaneous winds. Gas exchange is computed every 3 hours using wind speeds from the ECMWF operational model as represented by the **TM5 atmospheric transport model**. Other than the smooth trend in anthropogenic flux assumed by the OIF results, interannual variability (IAV) in the first guess ocean flux comes entirely from wind speed effects on the gas transfer velocity. This is because the ocean inversions retrieve only a long-term mean and smooth trend.

The initial release of CarbonTracker (2007A) used climatological estimates of CO₂ partial pressure in surface waters from Takahashi et al. [2002] to compute a first-guess air-sea flux. This air-sea pCO₂ disequilibrium was modulated by a surface barometric pressure correction before being multiplied by a gas-transfer coefficient to yield a flux. Starting with CarbonTracker 2007B and in this CarbonTracker Europe release, the air-sea pCO₂ disequilibrium is imposed from analysis of the OIF results, with short-term flux variability derived from the atmospheric model wind speeds via the gas transfer coefficient. The barometric pressure correction has been removed so that climatological high- and low-pressure cells do not bias the long-term means of the first guess fluxes. In either method, the first-guess fluxes have no interannual variability (IAV) due to pCO₂ changes, such as those that occur in the tropical eastern Pacific during an El Niño. In CarbonTracker, this flux IAV must be inferred from atmospheric CO₂ signals.

Air-sea transfer is inhibited by the presence of sea ice, and for this work fluxes are scaled by the daily sea ice fraction in each gridbox provided by the ECMWF forecast data.

The first-guess fluxes described here are subject to scaling during the CarbonTracker optimization process, in which atmospheric CO₂ mole fraction observations are combined with transport simulated by the atmospheric model to infer flux signals. In this process, signals of terrestrial flux in atmospheric CO₂ distribution can be erroneously interpreted as being caused by oceanic fluxes. This flux "aliasing" or "leakage" is evident in some regions as a change in the shape of the seasonal cycle of air-sea flux. Differences between CarbonTracker posterior air-sea fluxes and those of the OIF prior fluxes are minor, but do constitute an issue that we will be investigating in the future.

3. Further Reading

- **NOAA Pacific Marine Environmental Laboratory (PMEL)**
- **Ocean Acidification**
- Caldeira, K., and M. E. Wickett (2003), Anthropogenic carbon and ocean pH, *Nature*, 425365–365.
- Gloor, M., N. Gruber, J. Sarmiento, C. L. Sabine, R. A. Feely, and C. Rödenbeck (2003), A first estimate of present and preindustrial air-sea CO₂ flux patterns based on ocean interior carbon measurements and models, *Geophysical Research Letters*, 30, , 10.1029/2002GL015594.
- Gruber, N., J. L. Sarmiento, and T. F. Stocker (1996), An improved method for detecting anthropogenic CO₂ in the oceans, *Global Biogeochemical Cycles*, 10, , 809–837.
- Jacobson, A. R., N. Gruber, J. L. Sarmiento, M. Gloor, and S. E. Mikaloff Fletcher (2007), A joint atmosphere-ocean inversion for surface fluxes of carbon dioxide: I. Methods and global-scale fluxes, *Global Biogeochemical Cycles*, 21, doi:10.1029/2005GB002556.
- Pacanowski, R. C., and A. Gnanadesikan (1998), Transient response in a z-level ocean model that resolves topography with partial cells, *Monthly Weather Review*, 126, 3248–3270.
- Sabine, C. L., R. A. Feely, N. Gruber, R. M. Key, K. Lee, J. L. Bullister, R. Wanninkhof, C. S. Wong, D. W. R. Wallace, B. Tilbrook, F. J. Millero, T. H. Peng, A. Kozyr, T. Ono, and A. F. Rios (2004), The oceanic sink for anthropogenic CO₂, *Science*, 305, 367–371.
- Takahashi, T., S. C. Sutherland, C. Sweeney, A. P. N. Metzl, B. Tilbrook, N. Bates, R. Wanninkhof, R. A. Feely, C. Sabine, J. Olafsson, and Y. Nojiri (2002), Global air-sea CO₂ flux based on climatological surface ocean pCO₂, and seasonal biological and temperature effects, *Deep-Sea Research II*, 49, , 1601–1622.
- Wanninkhof, R. (1992), Relationship between wind speed and gas exchange over the ocean, *Journal of Geophysical Research*, 97, 7373–7382.

Fire Module [\[go to top\]](#)

1. Introduction

Vegetation fires are an important part of the carbon cycle and have been so for many millennia. Even before human civilization began to use fires to clear land for agricultural purposes, most ecosystems were subject to natural wildfires that would rejuvenate old forests and bring important minerals to the soils. When fires consume part of the landscape in either controlled or natural burning, carbon dioxide (amongst many other gases and aerosols) is released in large quantities. Each year, vegetation fires emit more than 2 PgC as CO₂ into the atmosphere, mostly in the tropics. Currently, a large fraction of these fires is started by humans, and mostly intentionally to clear land for agriculture, or to re-fertilize soils before a new growing season. This important component of the carbon cycle is monitored mostly from space, while sophisticated 'biomass burning' models are used to estimate the amount of CO₂ emitted by each fire. Such estimates are then used in CarbonTracker to prescribe the emissions, without further refinement by our measurements.

2. Detailed Description

The fire module currently used in CarbonTracker is based on the Global Fire Emissions Database version 4 (GFEDv4), which is used in the SiBCASA biosphere model as described [here](#). The GFED4 dataset consists of 0.25x0.25 degree gridded monthly burned area for the time period spanning January 1997 – August 2012. The CO₂ emissions are calculated in SiBCASA using the Burned Area and the vegetation types. The GFEDv4 burned area is based on MODIS satellite observations of fire counts. The full data set was produced by combining 500 m MODIS burned area maps with active fire data from the Tropical Rainfall Measuring Mission (TRMM) Visible and Infrared Scanner (VIRS) and the Along-Track Scanning Radiometer (ATSR) family of sensors.

Once burned area has been estimated globally, emissions of trace gases are calculated using the SiBCASA biosphere model. The seasonally changing vegetation and soil biomass stocks in the SiBCASA model are combusted based on the burned area estimate, and converted to atmospheric trace gases using estimates of fuel loads, combustion completeness, and burning efficiency. Between September 2012 and December 2013 we used climatological mean values.

GFED products were successfully used in recent studies of CH₄, CO₂, CO, and other trace gases.

3. Further Reading

- **Giglio, L. et al. (2013)**, Analysis of daily, monthly, and annual burned area using the fourth-generation global fire emissions database (GFED4), *J. Geophys. Res.: Biogeosciences*, 118, 317–328
- **van der Werf, G. R. et al. (2006)**, Interannual variability in global biomass burning emissions from 1997 to 2004, *Atm. Chem. Phys.*, 6(11), 3423–3441
- **van der Velde, I. R. et al. (2013)**, Biosphere model simulations of interannual variability in terrestrial ¹³C/¹²C exchange, *Global Biogeochemical Cycles*, 27(3), 637–649.
- **van der Velde, I. R. et al. (2014)**, Terrestrial cycling of ¹³CO₂ by photosynthesis, respiration, and biomass burning in SiBCASA, *Biogeosciences*, 11, 6553–6571.
- **Giglio et al. (2006)**, Global estimation of burned area using MODIS active fire observations, *Atmos. Chem. Phys.*, 6, 957–974

Biosphere Module [\[go to top\]](#)

1. Introduction

The biospheric component of the carbon cycle consists of all the carbon stored in 'biomass' around us. This includes trees, shrubs, grasses, carbon within soils, dead wood, and leaf litter. Such reservoirs of carbon can exchange CO₂ with the atmosphere. Exchange starts when plants take up CO₂ during their growing season through the process called photosynthesis (uptake). Most of this carbon is released back to the atmosphere throughout the year through a process called respiration (release). This includes both the decay of dead wood and litter and the metabolic respiration of living plants. Of course, plants can also return carbon to the atmosphere when they burn, **as described here**. Even though the yearly sum of uptake and release of carbon amounts to a relatively small number (a few petagrams (one Pg=10¹⁵ g)) of carbon per year, the flow of carbon each way is as large as 120 Pg each year. This is why the net result of these flows needs to be monitored in a system such as ours. It is also the reason we need a good physical description (model) of these flows of carbon. After all, from the atmospheric measurements we can only see the small net sum of the large two-way streams (gross fluxes). Information on what the biospheric fluxes are doing in each season, and in every location on Earth is derived from a specialized biosphere model, and fed into our system as a first guess, to be refined by our assimilation procedure.

2. Detailed Description

The biosphere model currently used in CarbonTracker is the Simple-Biosphere-Model-Carnegie-Ames Stanford Approach (SiBCASA) biogeochemical model. This model calculates global carbon fluxes using input from weather models to drive biophysical processes, as well as satellite observed Normalized Difference Vegetation Index (NDVI) to track plant phenology. The version of SiBCASA model output used so far was driven by year specific weather and satellite observations, and including the effects of fires on photosynthesis and respiration (see van der Velde et al., [2014], van der Werf et al., [2006] and Giglio et al., [2006]). This simulation gives 1x1 degree global fluxes on a 10-minute time resolution, which we average to monthly means for further processing.

3-Hourly Net Ecosystem Exchange (NEE) is derived directly from Gross Primary Production (GPP) and ecosystem respiration (R_e) from SiBCASA.

3. Further Reading

- **van der Velde, I. R. et al. (2013)**, Biosphere model simulations of interannual variability in terrestrial ¹³C/¹²C exchange, *Global Biogeochemical Cycles*, 27(3), 637–649.
- **van der Velde, I. R. et al. (2014)**, Terrestrial cycling of ¹³CO₂ by photosynthesis, respiration, and biomass burning in SiBCASA, *Biogeosciences*, 11, 6553–6571.
- **Schaefer, K. et al. (2008)**, Combined simple biosphere/Carnegie-Ames-Stanford approach terrestrial carbon cycle model. *Journal of Geophysical Research: Atmospheres*, 113(G3)
- **Olsen and Randerson (2004)**, Differences between surface and column atmospheric CO₂ and implications for carbon cycle research, *Journal of Geophysical Research: Atmospheres*, 109, D2, 27
- **van der Werf, G.R. et al. (2006)**, Interannual variability in global biomass burning emissions from 1997 to 2004, *Atm. Chem. Phys.*, 6(11), 3423–3441

Fossil Fuel Module [\[go to top\]](#)

1. Introduction

Human beings first influenced the carbon cycle through land-use change. Early humans used fire to control animals and later cleared forest for agriculture. Over the last two centuries, following the industrial and technical revolutions and the world population increase, fossil fuel combustion has become the largest anthropogenic source of CO₂. Coal, oil and natural gas combustion indeed are the most common energy sources in both developed and developing countries. Various sectors of the economy rely on fossil fuel combustion: power generation, transportation, residential/commercial building heating, and industrial processes. In 2014, the world emissions of CO₂ from fossil fuel burning, cement manufacturing, and flaring reached 9.8 PgC (one Pg=10¹⁵ grams of carbon) [CDIAC]. The largest share of CO₂ emissions to the atmosphere from fossil fuel burning was in China: 27% in 2014, followed by the USA (15%), Europe/EU28 (10%) and India (7%). CDIAC has projected that the global total source will slightly decrease in 2015, to 9.7 PgC.

2. Detailed Description

The fossil fuel emission inventory used in CarbonTracker Europe is the one constructed for the **CARBONES** project by **USTUTT/IER**. It uses emissions from the **EDGAR 4.2 database** together with country and sector specific time profiles derived by IER. A detailed description of the construction of the product is found [here](#). The global total emissions for 2010–2014 were scaled to the global totals used in the **Global Carbon Budget 2015**.

3. Further Reading

- **CDIAC (Marland et al.) Annual Global and National fluxes**
- **CDIAC (Blasing et al.) Monthly USA fluxes**
- **Energy Information Administration (EIA)**
- **CARBONES project**
- **EDGAR Database**
- **Institut für Energiewirtschaft und Rationelle Energieanwendung**

Observations [\[go to top\]](#)

1. Introduction

The observations of atmospheric CO₂ mole fraction by **different laboratories** are at the heart of CarbonTracker. They inform us on changes in the carbon cycle, whether they are regular (such as the seasonal growth and decay of leaves and trees), or irregular (such as the release of tons of carbon by a wildfire). The results in CarbonTracker depend directly on the quality, amount and location of observations available, and the degree of detail at which we can monitor the carbon cycle reliably increases strongly with the density of our observing network.

2. Detailed Description

This study uses CO₂ observations from in-situ measurements or from air samples collected in flasks at 147 global sites by several institutions worldwide. All contributing laboratories are included under **collaborators**. These observations are included in **ObsPack GLOBALVIEWplus1.0**. This ObsPack product contains 205 time series of surface flask samples, quasi-continuous in-situ observations also from towers and aircraft samples. Table 1 and the figure below summarize which time series have been used in our inversion. We assimilate a maximum of 1 time series per site (e.g. not 2 from the same location from different laboratories). Note that all of these observations are calibrated against the same world CO₂ scale (WMO-2007).

For most of the quasi-continuous sampling sites, the time series consist of hourly averaged mole fractions. We assimilate only mole fractions from the afternoon hours, recognizing that our atmospheric transport model does not always capture the continental nighttime stability regime while daytime well-mixed conditions are better matched. At mountain-top sites (e.g. MLO, NWR, and SPL), we use the mole fractions from the nighttime hours as this tends to be the most stable time period and avoids periods of upslope flows that contain local vegetative and/or anthropogenic influence. The selection of hourly observations included in the assimilation is based on the flags as set in the ObsPack data sets. A set of coastal sites is moved by one degree into the ocean to force the model sample to be more representative of the actual site conditions (based on Transcom continuous simulations). Table 1 summarizes how data from the different measurement programs are included for this study.

The CO₂ data from ObsPack used in CarbonTracker are freely available for **download**. Users are encouraged to review the literature and contact the measurement labs directly for details about and access to the actual observations.

We apply a further selection criterion during the assimilation to exclude non-marine boundary layer (MBL) and non-deep Southern Hemisphere observations that are very poorly forecasted in our framework. We use the so-called model–data mismatch (MDM) in this process, which is the random error ascribed to each observation to account for measurement errors as well as modeling errors of that observation. We scale the MDM with the amount of available observations per day, to represent both flask samples and quasi-continuous observations with equal weight. We interpret an observed–minus–forecasted (OmF) mole fraction that exceeds 3 times the prescribed model–data mismatch as an indicator that our modeling framework fails. This can happen for instance when an air sample is representative of local exchange not captured well by our 1x1 degree fluxes, when local meteorological conditions are not captured by our offline transport fields, but also when large-scale CO₂ exchange is suddenly changed (e.g. fires, pests, droughts) to an extent that can not be accommodated by our flux modules. This last situation would imply an important change in the carbon cycle and has to be recognized by the researchers when analyzing the results. In accordance with the 3–sigma rejection criterion, less than 1% of the observations are discarded through this mechanism in our assimilations.

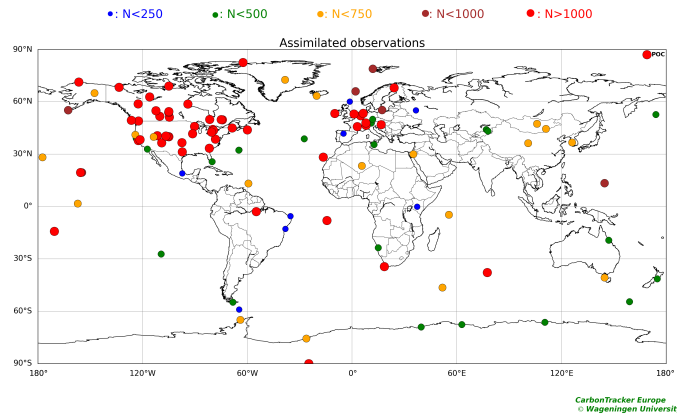


Table 1 gives a summary of the observing sites used in CarbonTracker and the assimilation performance. Model–data–mismatch ("R") is a value assigned to a given site that is meant to quantify our expected ability to simulate observations there. This value is principally determined from the limitations of the atmospheric transport model. It is part of the standard deviation used to interpret the difference between a simulation first guess ("Hx") of an observation and the actual measured value ("z"). The other component, HPH^T is a measure of the ability of the ensemble Kalman filter to improve its simulated value for this observation by adjusting fluxes. These elements together form the innovation χ statistic for the site: $\chi = (z - Hx) / \sqrt{(HPH^T + r^2)}$. The innovation χ^2 reported is the mean of all squared χ values for a given site. An average χ^2 below 1.0 indicates that the $\sqrt{(HPH^T + r^2)}$ values are too large. Conversely, values above 1.0 mean that this standard deviation is underestimated. The bias is a statistic of the posterior residuals (final modeled values – measured values). The bias is the mean of these residuals.

Table 1: Summary of observing sites used in CarbonTracker Europe and assimilation performance.

Site code	Sampling Type	Lab.	Country	Lat, Lon, Elev. (m ASL)	No. Obs. Available	No. Obs. Assimilated	\sqrt{R} ($\mu\text{mol mol}^{-3}$)	\sqrt{HPH} ($\mu\text{mol mol}^{-3}$)	H(x)–y ($\mu\text{mol mol}^{-3}$)	H(x)–y (JJAS) ($\mu\text{mol mol}^{-3}$)	H(x)–y (NDJFMA) ($\mu\text{mol mol}^{-3}$)	Inn. χ^2	Site code
ABP	surface-flask	NOAA	Brazil	12°46'S, 38°10'W, 1 masl	101	101	+1.50	+0.41	-0.77± 0.84	-0.30± 0.44	-1.26± 0.87	+0.59	ABP
ABP	surface-flask	IPEN	Brazil	12°46'S, 38°10'W, 1 masl	104	0	+1000.00	+0.43	-1.08± 1.45	-0.60± 1.44	-1.56± 1.29	-99.00	ABP
ABT	surface-insitu	EC	Canada	49° 2'N, 122°22'W, 100 masl	6765	802	+5.19	+13.11	-0.98± 4.19	-0.44± 4.07	-1.50± 4.37	+1.37	ABT
ACG	aircraft-pfp	NOAA	United States	Variable	1489	0	+1000.00	+1.17	+0.11± 1.78	+0.21± 2.05	+0.35± 1.23	-99.00	ACG
AIA	aircraft-flask	CSIRO	Australia	40°32'S, 144°18'E, 0 masl	63	0	+1000.00	+0.14	+0.23± 0.53	+0.23± 0.53	+nan± nan	-99.00	AIA
ALT	surface-flask	NOAA	Canada	82°27'N, 62°30'W, 200 masl	823	0	+1000.00	+0.48	+0.20± 0.77	+0.02± 0.96	+0.37± 0.65	-99.00	ALT
ALT	surface-flask	CSIRO	Canada	82°27'N, 62°30'W, 200 masl	509	0	+1000.00	+0.47	+0.25± 0.78	+0.10± 0.88	+0.45± 0.71	-99.00	ALT
ALT	surface-flask	SIO	Canada	82°27'N, 62°30'W, 200 masl	348	0	+1000.00	+0.49	+0.41± 0.75	+0.23± 0.89	+0.55± 0.68	-99.00	ALT
ALT	surface-insitu	EC	Canada	82°27'N, 62°30'W, 200 masl	111251	13786	+2.59	+0.47	+0.21± 0.76	+0.09± 0.90	+0.29± 0.71	+0.14	ALT
AMS	surface-insitu	LSCE	France	37°48'S, 77°32'E, 55 masl	4900	4900	+2.85	+0.26	-0.10± 0.46	+0.10± 0.36	-0.55± 0.41	+0.04	AMS
AMT	surface-pfp	NOAA	United States	45° 2'N, 68°41'W, 53 masl	914	0	+1000.00	+4.12	-0.12± 2.88	+0.29± 3.84	-0.34± 2.14	-99.00	AMT
AMT	tower-insitu	NOAA	United States	45° 2'N, 68°41'W, 53 masl	78736	12922	+7.83	+7.79	+0.06± 2.88	+0.48± 3.79	-0.21± 2.14	+0.17	AMT
AOA	aircraft-flask	JMA	Japan	Variable	1123	0	+1000.00	+0.17	+0.51± 1.01	+0.38± 1.21	+0.69± 0.89	-99.00	AOA
ARA	surface-flask	CSIRO	Australia	23°52'S, 148°28'E, 175 masl	22	0	+1000.00	+1.46	-1.10± 3.06	-0.06± 2.96	-0.29± 1.97	-99.00	ARA
ASC	surface-flask	NOAA	United Kingdom	7°58'S, 14°24'W, 85 masl	1269	1269	+0.75	+0.18	-0.07± 0.74	+0.25± 0.65	-0.33± 0.73	+1.05	ASC

Site code	Sampling Type	Lab.	Country	Lat, Lon, Elev. (m ASL)	No. Obs. Available	No. Obs. Assimilated	\sqrt{R} ($\mu\text{mol mol}^{-1}$)	$\sqrt{\text{HPH}}$ ($\mu\text{mol mol}^{-1}$)	H(x)-y ($\mu\text{mol mol}^{-1}$)	H(x)-y (JJAS) ($\mu\text{mol mol}^{-1}$)	H(x)-y (NDJFMA) ($\mu\text{mol mol}^{-1}$)	Inn. χ^2	Site code
ASK	surface-flask	NOAA	Algeria	23°16'N, 5°38'E, 2710 masl	655	655	+0.75	+0.13	+0.01± 0.59	-0.09± 0.57	+0.13± 0.60	+0.64	ASK
AZR	surface-flask	NOAA	Portugal	38°46'N, 27°23'W, 19 masl	400	396	+1.50	+0.45	+0.36± 1.29	+0.47± 1.42	+0.41± 1.23	+0.83	AZR
BAL	surface-flask	NOAA	Poland	55°21'N, 17°13'E, 3 masl	976	964	+5.02	+4.40	-0.61± 3.47	-0.91± 3.69	-0.34± 3.29	+0.47	BAL
BAO	surface-pfp	NOAA	United States	40° 3'N, 105° 0'W, 1584 masl	2134	0	+1000.00	+1.34	-1.22± 3.32	-1.09± 3.75	-1.42± 2.99	-99.00	BAO
BAO	tower-insitu	NOAA	United States	40° 3'N, 105° 0'W, 1584 masl	59794	9166	+5.89	+4.74	-1.30± 3.19	-1.01± 2.76	-1.63± 3.49	+0.39	BAO
BCK	surface-insitu	EC	Canada	62°48'N, 116° 3'W, 179 masl	33017	4113	+5.17	+3.21	+0.20± 1.85	+0.15± 2.65	+0.28± 1.24	+0.19	BCK
BGI	aircraft-pfp	NOAA	United States	42°49'N, 94°25'W, 355 masl	357	0	+1000.00	+2.77	+0.16± 2.50	+0.29± 3.32	+0.20± 1.45	-99.00	BGI
BHD	surface-flask	NOAA	New Zealand	41°24'S, 174°52'E, 85 masl	197	197	+0.75	+0.23	+0.18± 0.65	+0.50± 0.70	-0.05± 0.57	+0.96	BHD
BHD	surface-insitu	NIWA	New Zealand	41°24'S, 174°52'E, 85 masl	481	481	+0.79	+0.19	+0.28± 0.49	+0.45± 0.46	+0.12± 0.46	+0.58	BHD
BKT	surface-flask	NOAA	Indonesia	0°12'S, 100°19'E, 845 masl	319	0	+1000.00	+0.89	+3.00± 4.09	+2.90± 4.61	+3.14± 3.81	-99.00	BKT
BME	surface-flask	NOAA	United Kingdom	32°22'N, 64°39'W, 12 masl	236	230	+1.50	+0.54	+0.54± 1.26	+1.13± 1.21	+0.25± 1.28	+0.92	BME
BMW	surface-flask	NOAA	United Kingdom	32°16'N, 64°53'W, 30 masl	502	498	+1.51	+0.60	+0.63± 1.10	+0.62± 1.02	+0.62± 1.09	+0.77	BMW
BNE	aircraft-pfp	NOAA	United States	40°48'N, 97°11'W, 465 masl	1080	0	+1000.00	+2.27	+0.07± 3.40	+0.27± 3.81	+0.43± 1.66	-99.00	BNE
BRA	surface-insitu	EC	Canada	51°12'N, 104°42'W, 595 masl	32795	4125	+5.18	+6.86	-0.14± 2.40	+0.11± 3.29	-0.19± 2.00	+0.35	BRA
BRW	surface-flask	NOAA	United States	71°19'N, 156°37'W, 11 masl	864	0	+1000.00	+1.20	+0.13± 1.45	+0.12± 2.03	+0.18± 1.07	-99.00	BRW
Site code	Sampling Type	Lab.	Country	Lat, Lon, Elev. (m ASL)	No. Obs. Available	No. Obs. Assimilated	\sqrt{R} ($\mu\text{mol mol}^{-1}$)	$\sqrt{\text{HPH}}$ ($\mu\text{mol mol}^{-1}$)	H(x)-y ($\mu\text{mol mol}^{-1}$)	H(x)-y (JJAS) ($\mu\text{mol mol}^{-1}$)	H(x)-y (NDJFMA) ($\mu\text{mol mol}^{-1}$)	Inn. χ^2	Site code
BRW	surface-insitu	NOAA	United States	71°19'N, 156°37'W, 11 masl	119410	11190	+2.67	+1.43	+0.27± 0.76	+0.28± 1.00	+0.26± 0.65	+0.22	BRW
BSC	surface-flask	NOAA	Romania	44°11'N, 28°40'E, 0 masl	434	0	+1000.00	+4.01	-6.31± 9.28	-10.51±11.08	-3.98± 6.95	-99.00	BSC
CAR	aircraft-pfp	NOAA	United States	40°22'N, 104°18'W, 1740 masl	5102	0	+1000.00	+0.45	+0.41± 1.04	+0.20± 1.31	+0.60± 0.75	-99.00	CAR
CBA	surface-flask	NOAA	United States	55°13'N, 162°43'W, 21 masl	997	955	+1.51	+0.51	-0.33± 1.40	+0.57± 1.64	-0.77± 0.98	+1.02	CBA
CBA	surface-flask	SIO	United States	55°13'N, 162°43'W, 21 masl	313	0	+1000.00	+0.53	+0.19± 1.88	+1.14± 2.57	-0.21± 1.03	-99.00	CBA
CBY	surface-insitu	EC	Canada	69° 1'N, 105° 3'W, 35 masl	14337	1785	+5.16	+1.97	+0.42± 1.20	+0.33± 1.44	+0.47± 1.00	+0.10	CBY
CDL	surface-insitu	EC	Canada	53°59'N, 105° 7'W, 600 masl	66546	8260	+5.13	+9.79	+0.08± 2.11	+0.45± 2.85	-0.10± 1.64	+0.26	CDL
CES	tower-insitu	ECN	the Netherlands	51°58'N, 4°56'E, -1 masl	97340	0	+1000.00	+6.03	+1.75±10.01	+1.76± 9.89	+1.72±10.29	-99.00	CES
CES	tower-insitu	ECN	the Netherlands	51°58'N, 4°56'E, -1 masl	97269	15765	+5.87	+3.79	-0.04± 4.16	+0.56± 3.52	-0.51± 4.54	+0.72	CES
CES	tower-insitu	ECN	the Netherlands	51°58'N, 4°56'E, -1 masl	95578	0	+1000.00	+6.53	-3.44±13.66	-5.94±15.56	-1.96±12.48	-99.00	CES
CES	tower-insitu	ECN	the Netherlands	51°58'N, 4°56'E, -1 masl	96668	0	+1000.00	+6.31	-0.00±10.44	-0.43±10.14	+0.26±10.77	-99.00	CES
CFA	surface-flask	CSIRO	Australia	19°17'S, 147° 3'E, 2 masl	302	299	+1.64	+0.59	-0.54± 1.11	-0.12± 1.28	-0.85± 0.91	+0.56	CFA
CGO	surface-flask	NOAA	Australia	40°41'S, 144°41'E, 94 masl	517	517	+0.50	+0.12	+0.12± 0.35	+0.36± 0.29	-0.08± 0.29	+0.57	CGO
CGO	surface-flask	CSIRO	Australia	40°41'S, 144°41'E, 94 masl	762	0	+1000.00	+0.11	+0.10± 0.32	+0.31± 0.26	-0.08± 0.26	-99.00	CGO
CGO	surface-flask	SIO	Australia	40°41'S, 144°41'E, 94 masl	317	0	+1000.00	+0.12	+0.31± 0.34	+0.54± 0.30	+0.11± 0.26	-99.00	CGO
Site code	Sampling Type	Lab.	Country	Lat, Lon, Elev. (m ASL)	No. Obs. Available	No. Obs. Assimilated	\sqrt{R} ($\mu\text{mol mol}^{-1}$)	$\sqrt{\text{HPH}}$ ($\mu\text{mol mol}^{-1}$)	H(x)-y ($\mu\text{mol mol}^{-1}$)	H(x)-y (JJAS) ($\mu\text{mol mol}^{-1}$)	H(x)-y (NDJFMA) ($\mu\text{mol mol}^{-1}$)	Inn. χ^2	Site code
CHL	surface-insitu	EC	Canada	58°45'N, 94° 4'W, 29 masl	19945	2498	+5.16	+4.39	+0.18± 1.88	+0.20± 2.53	+0.27± 1.34	+0.17	CHL
CHM	surface-insitu	EC	Canada	49°41'N, 74°18'W, 393 masl	22635	2802	+5.18	+4.05	+0.07± 2.43	+0.74± 3.10	-0.27± 2.11	+0.28	CHM
CHR	surface-flask	NOAA	Republic of Kiribati	1°42'N, 157° 9'W, 0 masl	501	501	+0.75	+0.15	-0.42± 0.57	-0.27± 0.46	-0.50± 0.60	+0.98	CHR
CIB	surface-flask	NOAA	Spain	41°49'N, 4°56'W, 845 masl	255	243	+2.51	+2.96	+0.52± 2.34	+0.45± 2.59	+0.55± 1.98	+0.72	CIB
CMA	aircraft-pfp	NOAA	United States	38°50'N, 74°19'W, 0 masl	2039	0	+1000.00	+2.04	+0.33± 2.67	+0.08± 3.56	+0.46± 1.87	-99.00	CMA
CON	aircraft-flask	NIES	Multiple	Variable	3286	0	+1000.00	+0.14	-0.04± 0.76	+0.12± 0.67	-0.13± 0.78	-99.00	CON
CON	aircraft-insitu	NIES	Multiple	Variable	297018	0	+1000.00	+0.43	+0.06± 1.78	-0.45± 2.18	+0.18± 1.53	-99.00	CON
CPS	surface-insitu	EC	Canada	49°49'N, 74°59'W, 381 masl	26002	3251	+5.19	+4.42	+0.09± 2.39	+0.36± 3.22	-0.08± 1.63	+0.26	CPS
CPT	surface-flask	NOAA	South Africa	34°21'S, 18°29'E, 230 masl	190	0	+1000.00	+0.27	-0.17± 0.76	+0.00± 0.63	-0.36± 0.82	-99.00	CPT
CPT	surface-insitu	SAWS	South Africa	34°21'S, 18°29'E, 230 masl	99307	99307	+3.41	+0.29	+0.07± 0.58	+0.33± 0.54	-0.11± 0.53	+0.05	CPT
CRI	surface-flask	CSIRO	India	15° 5'N, 73°50'E, 60 masl	147	0	+1000.00	+6.21	-3.54± 6.78	-1.02± 4.21	-5.72± 7.75	-99.00	CRI
CRV	aircraft-pfp	NOAA	United States	64°59'N, 147°36'W, 611 masl	1447	0	+1000.00	+2.49	-1.31± 5.09	-1.68± 5.66	+0.12± 2.25	-99.00	CRV
CRV	surface-pfp	NOAA	United States	64°59'N, 147°36'W, 611 masl	584	573	+2.52	+2.01	+0.09± 1.98	+0.31± 2.62	-0.09± 1.37	+0.68	CRV
CRZ	surface-flask	NOAA	France	46°26'S, 51°51'E, 197 masl	569	569	+0.50	+0.14	+0.13± 0.30	+0.22± 0.27	+0.05± 0.30	+0.43	CRZ
CYA	surface-flask	CSIRO	Australia	66°17'S, 110°31'E, 47 masl	333	333	+0.58	+0.09	-0.05± 0.27	+0.11± 0.27	-0.15± 0.24	+0.27	CYA
Site code	Sampling Type	Lab.	Country	Lat, Lon, Elev. (m ASL)	No. Obs. Available	No. Obs. Assimilated	\sqrt{R} ($\mu\text{mol mol}^{-1}$)	$\sqrt{\text{HPH}}$ ($\mu\text{mol mol}^{-1}$)	H(x)-y ($\mu\text{mol mol}^{-1}$)	H(x)-y (JJAS) ($\mu\text{mol mol}^{-1}$)	H(x)-y (NDJFMA) ($\mu\text{mol mol}^{-1}$)	Inn. χ^2	Site code
DND	aircraft-pfp	NOAA	United States	47°30'N, 99°14'W, 472 masl	1702	0	+1000.00	+1.59	+0.21± 1.97	+0.24± 2.90	+0.31± 1.11	-99.00	DND
DRP	shipboard-flask	NOAA	N/A	59° 0'S, 64°41'W, 0 masl	182	182	+0.52	+0.20	+0.03± 0.36	+0.15± 0.38	-0.03± 0.33	+0.55	DRP
EGB	surface-insitu	EC	Canada	44°14'N, 79°47'W, 251 masl	74853	9334	+5.19	+9.78	+0.03± 2.97	+0.36± 3.44	-0.22± 2.61	+0.48	EGB

EIC	surface-flask	NOAA	Chile	27°10'S, 109°26'W, 47 masl	448	448	+1.50	+0.11	+0.35± 1.07	+0.82± 0.87	-0.05± 0.99	+0.57	EIC
ESP	aircraft-pfp	NOAA	Canada	49°23'N, 126°33'W, 7 masl	3279	0	+1000.00	+2.82	+0.07± 2.79	-0.14± 4.08	+0.22± 1.38	-99.00	ESP
ESP	surface-flask	CSIRO	Canada	49°23'N, 126°33'W, 7 masl	23	0	+1000.00	+0.88	+0.05± 1.29	+0.47± 0.67	-0.79± 1.35	-99.00	ESP
ESP	surface-insitu	EC	Canada	49°23'N, 126°33'W, 7 masl	44437	5530	+5.19	+3.87	+0.07± 2.03	+0.36± 2.34	+0.10± 1.64	+0.20	ESP
EST	surface-insitu	EC	Canada	51°40'N, 110°12'W, 707 masl	38993	4878	+5.18	+5.62	+0.03± 2.35	+0.49± 2.75	-0.18± 2.16	+0.31	EST
ETL	aircraft-pfp	NOAA	Canada	54°21'N, 104°59'W, 492 masl	2416	0	+1000.00	+1.28	+0.21± 1.63	+0.45± 2.29	+0.19± 1.06	-99.00	ETL
ETL	surface-insitu	EC	Canada	54°21'N, 104°59'W, 492 masl	75034	9356	+5.14	+7.27	+0.03± 1.95	+0.28± 2.58	-0.08± 1.50	+0.21	ETL
FNE	surface-insitu	EC	Canada	58°50'N, 122°34'W, 361 masl	3972	417	+5.20	+9.13	-0.74± 4.20	+0.19± 4.05	-1.10± 4.10	+1.21	FNE
FSD	surface-insitu	EC	Canada	49°53'N, 81°34'W, 210 masl	113321	14246	+5.14	+6.44	+0.19± 2.14	+0.57± 2.85	-0.01± 1.47	+0.25	FSD
FTL	aircraft-pfp	NOAA	Brazil	3°31'S, 38°17'W, 3 masl	160	0	+1000.00	+0.25	-0.48± 1.31	+0.13± 1.33	-1.03± 0.90	-99.00	FTL
FWI	aircraft-pfp	NOAA	United States	44°40'N, 90°58'W, 334 masl	378	0	+1000.00	+2.52	+0.03± 3.23	-0.27± 4.09	+0.73± 2.51	-99.00	FWI
GMI	surface-flask	NOAA	Guam	13°23'N, 144°39'E, 0 masl	924	924	+0.75	+0.09	+0.24± 0.82	+0.23± 0.91	+0.34± 0.70	+1.33	GMI
Site code	Sampling Type	Lab.	Country	Lat, Lon, Elev. (m ASL)	No. Obs. Available	No. Obs. Assimilated	√R (μmol mol⁻¹)	√HPH (μmol mol⁻¹)	H(x)-y (μmol mol⁻¹)	H(x)-y (JJAS) (μmol mol⁻¹)	H(x)-y (NDJFMA) (μmol mol⁻¹)	Inn. X²	Site code
GPA	surface-flask	CSIRO	Australia	12°15'S, 131° 3'E, 25 masl	51	0	+1000.00	+0.99	+1.20± 3.07	+1.15± 3.25	+1.20± 2.63	-99.00	GPA
HAA	aircraft-pfp	NOAA	United States	21°14'N, 158°57'W, 3 masl	1778	0	+1000.00	+0.11	+0.41± 0.81	+0.36± 0.85	+0.47± 0.73	-99.00	HAA
HBA	surface-flask	NOAA	United Kingdom	75°36'S, 26°13'W, 30 masl	647	647	+0.50	+0.13	+0.10± 0.25	+0.27± 0.23	-0.01± 0.21	+0.32	HBA
HDP	surface-insitu	NCAR	United States	40°34'N, 111°39'W, 3351 masl	53195	53194	+7.01	+0.36	-0.15± 1.23	-0.29± 1.50	-0.10± 1.03	+0.04	HDP
HEI	surface-insitu	UHEI-IUP	Germany	49°25'N, 8°40'E, 116 masl	100021	0	+1000.00	+7.15	-7.47±14.93	-7.72±13.23	-7.30±16.09	-99.00	HEI
HFM	aircraft-pfp	NOAA	United States	42°32'N, 72°10'W, 340 masl	1609	0	+1000.00	+2.10	+0.43± 2.66	+0.22± 3.77	+0.34± 1.57	-99.00	HFM
HIL	aircraft-pfp	NOAA	United States	40° 4'N, 87°55'W, 201 masl	2065	0	+1000.00	+2.28	-0.27± 2.95	-0.68± 4.23	+0.08± 1.75	-99.00	HIL
HIP	aircraft-insitu	HU	United States	Variable	130016	0	+1000.00	+0.47	+0.04± 1.24	+0.18± 1.32	-0.10± 1.13	-99.00	HIP
HNP	surface-insitu	EC	Canada	43°37'N, 79°23'W, 87 masl	4318	510	+5.19	+13.10	+0.43± 3.56	+0.08± 4.05	+0.57± 3.09	+0.72	HNP
HPB	surface-flask	NOAA	Germany	47°48'N, 11° 1'E, 936 masl	379	372	+5.00	+4.33	+1.25± 4.10	+1.94± 4.06	+0.72± 4.06	+0.75	HPB
HUN	surface-flask	NOAA	Hungary	46°57'N, 16°39'E, 248 masl	702	0	+1000.00	+7.08	-0.29± 5.26	+0.34± 4.38	-0.59± 6.02	-99.00	HUN
HUN	tower-insitu	HMS	Hungary	46°57'N, 16°39'E, 248 masl	108610	0	+1000.00	+10.93	-7.59±16.51	-12.35±21.61	-3.73±10.42	-99.00	HUN
HUN	tower-insitu	HMS	Hungary	46°57'N, 16°39'E, 248 masl	109990	17870	+5.98	+9.89	+0.03± 3.66	+0.48± 3.29	-0.23± 3.90	+0.63	HUN
HUN	tower-insitu	HMS	Hungary	46°57'N, 16°39'E, 248 masl	112023	0	+1000.00	+10.57	-2.73± 9.93	-4.32±11.88	-1.25± 8.04	-99.00	HUN
HUN	tower-insitu	HMS	Hungary	46°57'N, 16°39'E, 248 masl	108599	0	+1000.00	+10.18	-0.89± 8.42	-1.48± 9.82	-0.21± 7.20	-99.00	HUN
Site code	Sampling Type	Lab.	Country	Lat, Lon, Elev. (m ASL)	No. Obs. Available	No. Obs. Assimilated	√R (μmol mol⁻¹)	√HPH (μmol mol⁻¹)	H(x)-y (μmol mol⁻¹)	H(x)-y (JJAS) (μmol mol⁻¹)	H(x)-y (NDJFMA) (μmol mol⁻¹)	Inn. X²	Site code
ICE	surface-flask	NOAA	Iceland	63°24'N, 20°17'W, 118 masl	656	656	+0.75	+0.41	-0.44± 1.20	-0.15± 1.19	-0.58± 1.16	+3.05	ICE
INU	surface-insitu	EC	Canada	68°19'N, 133°32'W, 113 masl	24741	3094	+5.19	+3.59	+0.08± 1.82	+0.24± 2.33	+0.03± 1.40	+0.18	INU
INX	aircraft-pfp	NOAA	United States	Variable	250	0	+1000.00	+5.14	-1.70± 5.44	-2.79± 7.64	-1.60± 4.43	-99.00	INX
INX	surface-pfp	NOAA	United States	Variable	1127	0	+1000.00	+8.08	-0.25± 9.33	+0.71±12.42	-1.06± 7.31	-99.00	INX
IZO	surface-flask	NOAA	Spain	28°19'N, 16°30'W, 2372 masl	594	0	+1000.00	+0.15	+0.63± 0.99	+0.60± 0.95	+0.67± 1.02	-99.00	IZO
IZO	surface-insitu	AEMET	Spain	28°19'N, 16°30'W, 2372 masl	107971	56648	+2.56	+0.15	+0.10± 0.76	+0.05± 0.82	+0.14± 0.76	+0.10	IZO
JFJ	surface-insitu	KUP	Switzerland	46°33'N, 7°59'E, 3570 masl	72846	12076	+2.99	+0.77	+0.32± 1.64	+0.50± 1.45	+0.18± 1.78	+0.36	JFJ
JFJ	surface-insitu	EMPA	Switzerland	46°33'N, 7°59'E, 3570 masl	31585	5236	+2.96	+0.79	+0.30± 1.42	+0.37± 1.26	+0.24± 1.52	+0.31	JFJ
KAS	surface-insitu	AGH	Poland	49°14'N, 19°59'E, 1989 masl	77012	0	+1000.00	+1.54	+0.01± 4.94	+2.15± 4.96	-1.62± 4.30	-99.00	KAS
KEY	surface-flask	NOAA	United States	25°40'N, 80° 9'W, 1 masl	498	494	+1.50	+0.79	+0.09± 0.92	+0.25± 0.83	-0.04± 1.01	+0.40	KEY
KUM	surface-flask	NOAA	United States	19°31'N, 154°49'W, 3 masl	902	902	+0.89	+0.11	-0.01± 0.97	-0.07± 1.01	+0.09± 0.98	+1.34	KUM
KUM	surface-flask	SIO	United States	19°31'N, 154°49'W, 3 masl	507	0	+1000.00	+0.11	+0.06± 1.14	+0.03± 1.17	+0.13± 1.21	-99.00	KUM
KZD	surface-flask	NOAA	Kazakhstan	44° 5'N, 76°52'E, 595 masl	441	426	+2.50	+2.25	-0.32± 2.47	-0.86± 2.76	+0.01± 2.06	+1.03	KZD
KZM	surface-flask	NOAA	Kazakhstan	43°15'N, 77°53'E, 2519 masl	393	392	+2.50	+0.89	+0.20± 2.22	+0.86± 2.11	-0.54± 1.83	+0.84	KZM
LEF	aircraft-pfp	NOAA	United States	45°57'N, 90°16'W, 472 masl	2967	0	+1000.00	+2.73	-0.03± 2.39	-0.06± 3.31	+0.15± 1.52	-99.00	LEF
Site code	Sampling Type	Lab.	Country	Lat, Lon, Elev. (m ASL)	No. Obs. Available	No. Obs. Assimilated	√R (μmol mol⁻¹)	√HPH (μmol mol⁻¹)	H(x)-y (μmol mol⁻¹)	H(x)-y (JJAS) (μmol mol⁻¹)	H(x)-y (NDJFMA) (μmol mol⁻¹)	Inn. X²	Site code
LEF	surface-pfp	NOAA	United States	45°57'N, 90°16'W, 472 masl	2448	0	+1000.00	+4.53	-0.11± 3.66	+0.33± 5.30	-0.19± 2.26	-99.00	LEF
LEF	tower-insitu	NOAA	United States	45°57'N, 90°16'W, 472 masl	115810	19169	+5.98	+4.40	+0.09± 2.39	+0.41± 3.07	-0.07± 1.80	+0.26	LEF
LJO	surface-flask	SIO	United States	32°52'N, 117°15'W, 10 masl	307	303	+5.03	+0.84	+4.12± 2.61	+5.79± 2.80	+3.14± 1.99	+1.00	LJO
LLB	surface-flask	NOAA	Canada	54°57'N, 112°27'W, 540 masl	159	0	+1000.00	+4.91	+0.12± 5.00	+0.95± 5.82	-0.14± 4.87	-99.00	LLB
LLB	surface-insitu	EC	Canada	54°57'N, 112°27'W, 540 masl	59417	7351	+5.16	+6.95	-0.37± 2.97	+0.20± 3.38	-0.62± 2.72	+0.50	LLB
LMP	surface-flask	NOAA	Italy	35°31'N, 12°37'E, 45 masl	337	331	+1.50	+1.35	+0.53± 1.36	+0.04± 1.45	+0.86± 1.18	+0.99	LMP
LUT	surface-insitu	RUG	Netherlands	53°24'N, 6°21'E, 1 masl	51843	8651	+9.91	+6.64	-0.55± 4.76	-0.05± 4.22	-0.81± 5.04	+0.33	LUT

MAA	surface-flask	CSIRO	Australia	67°37'S, 62°52'E, 32 masl	356	356	+0.58	+0.09	-0.03± 0.29	+0.16± 0.28	-0.16± 0.23	+0.30	MAA
MEX	surface-flask	NOAA	Mexico	18°59'N, 97°19'W, 4464 masl	242	242	+2.50	+0.40	+0.83± 1.59	+1.49± 1.58	+0.22± 1.13	+0.50	MEX
MHD	surface-flask	NOAA	Ireland	53°20'N, 9°54'W, 5 masl	585	580	+1.50	+0.69	+0.33± 0.97	+0.66± 1.08	+0.15± 0.92	+0.50	MHD
MHD	surface-insitu	LSCE	Ireland	53°20'N, 9°54'W, 5 masl	41109	41050	+7.28	+1.53	-0.22± 2.75	-0.15± 3.51	-0.26± 2.11	+0.19	MHD
MID	surface-flask	NOAA	United States	28°13'N, 177°23'W, 11 masl	686	686	+1.50	+0.21	+0.63± 0.92	+0.97± 0.97	+0.50± 0.89	+0.60	MID
MKN	surface-flask	NOAA	Kenya	0° 4'S, 37°18'E, 3644 masl	138	138	+2.50	+0.22	+1.65± 1.95	+2.35± 2.23	+1.32± 1.50	+1.04	MKN
MLO	surface-flask	NOAA	United States	19°32'N, 155°35'W, 3397 masl	1090	0	+1000.00	+0.11	+0.13± 0.59	+0.05± 0.65	+0.21± 0.56	-99.00	MLO
MLO	surface-flask	CSIRO	United States	19°32'N, 155°35'W, 3397 masl	483	0	+1000.00	+0.10	+0.20± 0.67	+0.00± 0.55	+0.41± 0.73	-99.00	MLO
Site code	Sampling Type	Lab.	Country	Lat, Lon, Elev. (m ASL)	No. Obs. Available	No. Obs. Assimilated	√R (μmol mol ⁻¹)	√HPH (μmol mol ⁻¹)	H(x)-y (μmol mol ⁻¹)	H(x)-y (JJAS) (μmol mol ⁻¹)	H(x)-y (NDJFMA) (μmol mol ⁻¹)	Inn. X ²	Site code
MLO	surface-flask	SIO	United States	19°32'N, 155°35'W, 3397 masl	558	0	+1000.00	+0.10	+0.29± 0.64	+0.14± 0.59	+0.41± 0.70	-99.00	MLO
MLO	surface-insitu	NOAA	United States	19°32'N, 155°35'W, 3397 masl	119104	14714	+1.42	+0.10	+0.19± 0.55	-0.06± 0.49	+0.36± 0.54	+0.21	MLO
MNM	surface-insitu	JMA	Japan	24°17'N, 153°59'E, 8 masl	102234	0	+1000.00	+0.21	+0.30± 0.76	+0.22± 0.80	+0.47± 0.73	-99.00	MNM
MQA	surface-flask	CSIRO	Australia	54°29'S, 158°58'E, 6 masl	440	440	+0.58	+0.14	+0.04± 0.38	+0.23± 0.39	-0.08± 0.33	+0.51	MQA
NAT	surface-flask	NOAA	Brazil	5°31'S, 35°16'W, 15 masl	171	171	+2.50	+0.15	-0.64± 1.05	-0.56± 1.07	-0.71± 1.04	+0.25	NAT
NAT	surface-flask	IPEN	Brazil	5°31'S, 35°16'W, 15 masl	89	0	+1000.00	+0.14	-0.52± 1.19	-0.45± 1.23	-0.48± 1.20	-99.00	NAT
NHA	aircraft-pfp	NOAA	United States	42°57'N, 70°38'W, 0 masl	2910	0	+1000.00	+1.83	+0.38± 2.42	+0.48± 3.41	+0.36± 1.83	-99.00	NHA
NMB	surface-flask	NOAA	Namibia	23°35'S, 15° 2'E, 456 masl	295	295	+1.50	+0.54	-0.24± 1.05	+0.21± 1.01	-0.73± 0.90	+0.60	NMB
NWR	surface-flask	NOAA	United States	40° 3'N, 105°35'W, 3523 masl	669	0	+1000.00	+0.47	+0.54± 1.22	+1.29± 1.35	+0.16± 0.90	-99.00	NWR
NWR	surface-insitu	NCAR	United States	40° 3'N, 105°35'W, 3523 masl	61718	61717	+11.67	+0.49	+0.12± 1.41	+0.19± 1.84	+0.17± 1.09	+0.02	NWR
NWR	surface-pfp	NOAA	United States	40° 3'N, 105°35'W, 3523 masl	1841	0	+1000.00	+0.56	+0.76± 1.76	+1.37± 2.27	+0.41± 1.21	-99.00	NWR
OBN	surface-flask	NOAA	Russia	55° 7'N, 36°36'E, 183 masl	133	133	+5.03	+3.63	+0.13± 3.70	-0.66± 4.09	+0.77± 3.56	+0.60	OBN
OIL	aircraft-pfp	NOAA	United States	41°17'N, 88°56'W, 192 masl	424	0	+1000.00	+2.14	+0.64± 2.28	+0.71± 3.04	+0.44± 1.36	-99.00	OIL
OTA	surface-flask	CSIRO	Australia	38°31'S, 142°49'E, 40 masl	139	0	+1000.00	+0.30	-1.43±19.80	-1.72±13.00	+2.49±17.59	-99.00	OTA
OKX	surface-flask	NOAA	Germany	50° 2'N, 11°49'E, 1009 masl	319	319	+5.00	+1.74	-0.07± 3.58	+0.41± 3.83	-0.73± 3.41	+0.55	OKX
Site code	Sampling Type	Lab.	Country	Lat, Lon, Elev. (m ASL)	No. Obs. Available	No. Obs. Assimilated	√R (μmol mol ⁻¹)	√HPH (μmol mol ⁻¹)	H(x)-y (μmol mol ⁻¹)	H(x)-y (JJAS) (μmol mol ⁻¹)	H(x)-y (NDJFMA) (μmol mol ⁻¹)	Inn. X ²	Site code
PAL	surface-flask	NOAA	Finland	67°58'N, 24° 7'E, 560 masl	541	0	+1000.00	+2.54	-0.12± 2.43	+0.11± 3.10	-0.18± 2.01	-99.00	PAL
PAL	surface-insitu	FMI	Finland	67°58'N, 24° 7'E, 560 masl	25459	0	+1000.00	+2.89	-0.16± 2.17	+0.07± 2.86	-0.16± 1.97	-99.00	PAL
PAL	surface-insitu	FMI	Finland	67°58'N, 24° 7'E, 560 masl	22553	0	+1000.00	+1.46	+0.12± 1.22	+0.49± 1.66	+0.01± 0.98	-99.00	PAL
PAL	surface-insitu	FMI	Finland	67°58'N, 24° 7'E, 560 masl	84326	84323	+10.73	+2.44	+0.01± 1.86	+0.36± 2.43	-0.09± 1.59	+0.05	PAL
PFA	aircraft-pfp	NOAA	United States	65° 4'N, 147°17'W, 210 masl	3523	0	+1000.00	+1.01	+0.16± 1.68	+0.44± 2.40	+0.12± 1.19	-99.00	PFA
POC	shipboard-flask	NOAA	N/A	Variable	2169	2164	+0.88	+0.27	-0.02± 1.67	-0.02± 1.51	-0.02± 1.74	+4.67	POC
PSA	surface-flask	NOAA	United States	64°55'S, 64° 0'W, 10 masl	722	722	+0.50	+0.27	-0.01± 0.31	+0.07± 0.30	-0.04± 0.28	+0.40	PSA
PSA	surface-flask	SIO	United States	64°55'S, 64° 0'W, 10 masl	350	0	+1000.00	+0.27	+0.17± 0.34	+0.30± 0.28	+0.09± 0.33	-99.00	PSA
PTA	surface-flask	NOAA	United States	38°57'N, 123°44'W, 17 masl	398	394	+5.01	+2.65	-2.35± 3.46	-1.81± 3.38	-2.44± 3.50	+0.70	PTA
PUY	surface-insitu	LSCE	France	45°46'N, 2°58'E, 1465 masl	24990	4167	+4.99	+2.47	-0.75± 2.77	-0.74± 3.22	-0.74± 2.21	+0.42	PUY
RBA	surface-insitu	NCAR	United States	36°28'N, 109° 6'W, 2982 masl	20181	20181	+11.77	+0.36	+0.17± 1.02	-0.09± 1.25	+0.33± 0.83	+0.01	RBA
RPB	surface-flask	NOAA	Barbados	13°10'N, 59°26'W, 15 masl	690	690	+1.50	+0.29	+0.00± 0.69	+0.46± 0.63	-0.20± 0.58	+0.22	RPB
RTA	aircraft-pfp	NOAA	Cook Islands	21°15'S, 159°50'W, 3 masl	2194	0	+1000.00	+0.11	-0.13± 0.68	+0.15± 0.49	-0.35± 0.74	-99.00	RTA
RYO	surface-insitu	JMA	Japan	39° 2'N, 141°49'E, 260 masl	62540	0	+1000.00	+1.33	-0.35± 2.35	+0.28± 3.63	-0.27± 1.68	-99.00	RYO
SAN	aircraft-pfp	NOAA	Brazil	2°51'S, 54°57'W, 78 masl	322	322	+8.00	+0.58	-0.06± 2.77	-1.09± 2.91	+0.79± 2.70	+0.13	SAN
Site code	Sampling Type	Lab.	Country	Lat, Lon, Elev. (m ASL)	No. Obs. Available	No. Obs. Assimilated	√R (μmol mol ⁻¹)	√HPH (μmol mol ⁻¹)	H(x)-y (μmol mol ⁻¹)	H(x)-y (JJAS) (μmol mol ⁻¹)	H(x)-y (NDJFMA) (μmol mol ⁻¹)	Inn. X ²	Site code
SAN	aircraft-pfp	IPEN	Brazil	2°51'S, 54°57'W, 78 masl	1641	1641	+8.13	+0.59	-0.21± 2.38	-0.33± 2.61	-0.06± 2.26	+0.09	SAN
SCA	aircraft-pfp	NOAA	United States	32°46'N, 79°33'W, 0 masl	2288	0	+1000.00	+1.24	+0.13± 2.12	-0.03± 2.51	+0.15± 1.91	-99.00	SCA
SCT	surface-pfp	NOAA	United States	33°24'N, 81°50'W, 115 masl	1453	0	+1000.00	+4.15	-0.32± 3.89	-0.20± 3.97	-0.58± 3.98	-99.00	SCT
SCT	tower-insitu	NOAA	United States	33°24'N, 81°50'W, 115 masl	51664	8565	+5.98	+5.46	+0.17± 3.31	+0.20± 3.83	+0.00± 2.97	+0.44	SCT
SEY	surface-flask	NOAA	Seychelles	4°41'S, 55°32'E, 2 masl	644	644	+0.75	+0.18	-0.15± 0.75	+0.04± 0.53	-0.36± 0.87	+1.10	SEY
SGP	aircraft-pfp	NOAA	United States	36°36'N, 97°29'W, 314 masl	5157	0	+1000.00	+2.37	+0.21± 2.37	-0.17± 2.79	+0.57± 1.62	-99.00	SGP
SGP	surface-flask	NOAA	United States	36°36'N, 97°29'W, 314 masl	584	561	+3.00	+4.64	-0.10± 2.33	-0.46± 2.74	+0.17± 2.04	+0.57	SGP
SGP	surface-insitu	LBNL-ARM	United States	36°36'N, 97°29'W, 314 masl	81033	13360	+5.98	+9.96	+0.06± 2.68	-0.09± 3.03	+0.09± 2.41	+0.34	SGP
SHM	surface-flask	NOAA	United States	52°43'N, 174° 8'E, 23 masl	492	490	+2.50	+0.51	+0.08± 1.96	+1.76± 2.22	-0.86± 1.04	+0.74	SHM
SIS	surface-flask	CSIRO	Scotland	60° 5'N, 1°15'W, 30 masl	89	88	+1.51	+0.45	+0.67± 0.95	+1.40± 1.01	+0.21± 0.67	+0.77	SIS
SMO	surface-flask	NOAA	American Samoa	14°15'S, 170°34'W, 42 masl	1161	0	+1000.00	+0.11	-0.18± 0.57	+0.17± 0.38	-0.51± 0.53	-99.00	SMO

SMO	surface-flask	SIO	American Samoa	14°15'S, 170°34'W, 42 masl	408	0	+1000.00	+0.11	-0.13± 0.74	+0.19± 0.68	-0.41± 0.71	-99.00	SMO
SMO	surface-insitu	NOAA	American Samoa	14°15'S, 170°34'W, 42 masl	114758	15361	+1.41	+0.10	-0.12± 0.52	+0.25± 0.35	-0.46± 0.45	+0.18	SMO
SNP	tower-insitu	NOAA	United States	38°37'N, 78°21'W, 1008 masl	45495	7504	+7.97	+3.61	+0.13± 4.20	+1.99± 4.87	-1.00± 3.38	+0.41	SNP
SPL	surface-insitu	NCAR	United States	40°27'N, 106°44'W, 3210 masl	61206	61200	+6.99	+0.51	-0.42± 1.62	-0.19± 2.04	-0.60± 1.32	+0.07	SPL
Site code	Sampling Type	Lab.	Country	Lat, Lon, Elev. (m ASL)	No. Obs. Available	No. Obs. Assimilated	√R (μmol mol ⁻¹)	√HPH (μmol mol ⁻¹)	H(x)-y (μmol mol ⁻¹)	H(x)-y (JJAS) (μmol mol ⁻¹)	H(x)-y (NDJFMA) (μmol mol ⁻¹)	Inn. X ²	Site code
SPO	surface-flask	NOAA	United States	89°59'S, 24°48'W, 2810 masl	774	0	+1000.00	+0.08	+0.11± 0.27	+0.35± 0.20	-0.05± 0.21	-99.00	SPO
SPO	surface-flask	CSIRO	United States	89°59'S, 24°48'W, 2810 masl	147	0	+1000.00	+0.08	-0.04± 0.26	+0.14± 0.25	-0.18± 0.20	-99.00	SPO
SPO	surface-flask	SIO	United States	89°59'S, 24°48'W, 2810 masl	346	0	+1000.00	+0.09	+0.13± 0.28	+0.36± 0.23	-0.03± 0.22	-99.00	SPO
SPO	surface-insitu	NOAA	United States	89°59'S, 24°48'W, 2810 masl	122079	20070	+0.98	+0.09	+0.03± 0.26	+0.25± 0.20	-0.13± 0.19	+0.08	SPO
SSL	surface-insitu	UBA-SCHAU	Germany	47°55'N, 7°55'E, 1205 masl	121836	20192	+4.99	+2.75	-0.56± 2.86	-0.57± 3.25	-0.43± 2.55	+0.51	SSL
STM	surface-flask	NOAA	Norway	66° 0'N, 2° 0'E, 0 masl	853	850	+1.50	+0.86	+0.23± 1.03	+0.45± 1.07	+0.13± 0.98	+0.60	STM
STR	surface-pfp	NOAA	United States	37°45'N, 122°27'W, 254 masl	3043	1365	+3.04	+1.94	+0.08± 2.26	+0.29± 2.39	-0.04± 2.23	+0.53	STR
SUM	surface-flask	NOAA	Greenland	72°36'N, 38°25'W, 3209 masl	624	624	+0.75	+0.24	+0.25± 0.73	+0.45± 0.82	+0.14± 0.68	+1.17	SUM
SYO	surface-flask	NOAA	Japan	69° 1'S, 39°35'E, 14 masl	347	347	+0.50	+0.10	-0.01± 0.26	+0.18± 0.23	-0.14± 0.21	+0.31	SYO
SYO	surface-insitu	TU	Japan	69° 1'S, 39°35'E, 14 masl	5419	0	+1000.00	+0.10	-0.04± 0.23	+0.13± 0.22	-0.14± 0.19	-99.00	SYO
TAP	surface-flask	NOAA	Republic of Korea	36°44'N, 126° 8'E, 16 masl	597	595	+5.50	+1.65	-0.02± 3.51	+0.82± 4.38	-0.37± 2.62	+0.46	TAP
TGC	aircraft-pfp	NOAA	United States	27°44'N, 96°52'W, 0 masl	2086	0	+1000.00	+0.75	+0.23± 1.43	+0.18± 1.36	+0.37± 1.37	-99.00	TGC
THD	aircraft-pfp	NOAA	United States	41° 3'N, 124° 9'W, 107 masl	1591	0	+1000.00	+2.03	+0.23± 2.55	-0.07± 2.24	+0.46± 2.73	-99.00	THD
THD	surface-flask	NOAA	United States	41° 3'N, 124° 9'W, 107 masl	565	562	+5.09	+2.20	-1.90± 3.51	-2.34± 3.89	-1.46± 3.09	+0.64	THD
TPD	surface-insitu	EC	Canada	42°37'N, 80°33'W, 231 masl	18132	2219	+5.19	+14.92	+0.16± 3.06	+0.34± 3.99	+0.07± 2.37	+0.61	TPD
Site code	Sampling Type	Lab.	Country	Lat, Lon, Elev. (m ASL)	No. Obs. Available	No. Obs. Assimilated	√R (μmol mol ⁻¹)	√HPH (μmol mol ⁻¹)	H(x)-y (μmol mol ⁻¹)	H(x)-y (JJAS) (μmol mol ⁻¹)	H(x)-y (NDJFMA) (μmol mol ⁻¹)	Inn. X ²	Site code
ULB	aircraft-pfp	NOAA	Mongolia	47°24'N, 106° 0'E, 1350 masl	517	517	+6.67	+0.71	+0.42± 1.59	+0.85± 2.20	+0.38± 1.29	+0.07	ULB
USH	surface-flask	NOAA	Argentina	54°51'S, 68°19'W, 12 masl	351	351	+0.75	+0.17	-0.26± 0.55	-0.27± 0.46	-0.18± 0.57	+0.66	USH
UTA	surface-flask	NOAA	United States	39°54'N, 113°43'W, 1327 masl	649	646	+2.50	+1.62	+0.29± 1.89	+0.81± 1.99	-0.19± 1.65	+0.63	UTA
UUM	surface-flask	NOAA	Mongolia	44°27'N, 111° 6'E, 1007 masl	690	656	+2.50	+1.06	-0.16± 2.48	-0.64± 2.70	+0.31± 2.09	+1.09	UUM
WAO	surface-insitu	UEA	United Kingdom	52°57'N, 1° 7'E, 20 masl	23679	3785	+9.60	+4.64	+0.93± 4.36	+0.80± 4.82	+1.14± 4.05	+0.29	WAO
WBI	aircraft-pfp	NOAA	United States	41°43'N, 91°21'W, 241 masl	1644	0	+1000.00	+2.77	+0.15± 2.43	-0.33± 3.22	+0.50± 1.43	-99.00	WBI
WBI	surface-pfp	NOAA	United States	41°43'N, 91°21'W, 241 masl	1785	0	+1000.00	+6.38	-0.47± 3.93	-0.71± 5.34	-0.35± 2.68	-99.00	WBI
WBI	tower-insitu	NOAA	United States	41°43'N, 91°21'W, 241 masl	58271	9566	+5.98	+5.82	+0.02± 3.17	+0.33± 4.14	-0.21± 2.45	+0.51	WBI
WGC	surface-pfp	NOAA	United States	38°16'N, 121°29'W, 0 masl	1683	0	+1000.00	+8.71	-2.08± 9.09	+1.13± 8.49	-4.22± 9.33	-99.00	WGC
WGC	tower-insitu	NOAA	United States	38°16'N, 121°29'W, 0 masl	57897	9467	+5.99	+4.76	+0.17± 3.57	+1.09± 2.86	-0.21± 3.93	+0.51	WGC
WIS	surface-flask	NOAA	Israel	29°58'N, 35° 3'E, 151 masl	738	735	+2.50	+0.48	-0.16± 1.94	+0.34± 1.65	-0.32± 1.96	+0.62	WIS
WKT	surface-pfp	NOAA	United States	31°19'N, 97°20'W, 251 masl	1874	0	+1000.00	+3.29	-0.35± 2.91	-0.46± 3.12	-0.25± 2.65	-99.00	WKT
WKT	tower-insitu	NOAA	United States	31°19'N, 97°20'W, 251 masl	89352	14774	+5.98	+2.97	+0.03± 2.48	-0.04± 2.41	+0.07± 2.51	+0.24	WKT
WLG	surface-flask	NOAA	Peoples Republic of China	36°17'N, 100°54'E, 3810 masl	589	576	+1.53	+0.90	+0.04± 1.40	+0.19± 1.46	+0.21± 1.32	+0.89	WLG
WSA	surface-insitu	EC	Canada	43°56'N, 60° 1'W, 5 masl	87000	10873	+5.19	+1.71	+0.26± 2.12	+0.84± 2.71	+0.02± 1.68	+0.22	WSA
Site code	Sampling Type	Lab.	Country	Lat, Lon, Elev. (m ASL)	No. Obs. Available	No. Obs. Assimilated	√R (μmol mol ⁻¹)	√HPH (μmol mol ⁻¹)	H(x)-y (μmol mol ⁻¹)	H(x)-y (JJAS) (μmol mol ⁻¹)	H(x)-y (NDJFMA) (μmol mol ⁻¹)	Inn. X ²	Site code
YON	surface-insitu	JMA	Japan	24°28'N, 123° 1'E, 30 masl	78139	0	+1000.00	+0.39	+0.03± 1.74	+0.22± 1.60	+0.14± 1.74	-99.00	YON
ZEP	surface-flask	NOAA	Norway and Sweden	78°54'N, 11°53'E, 474 masl	757	754	+1.50	+0.48	+0.33± 0.88	+0.49± 0.92	+0.17± 0.88	+0.53	ZEP

3. Further Reading

- [ESRL Carbon Cycle Program](#)
- [WMO/GAW Report No. 206, 2012](#) [Note: Requires a few minutes to load]
- [ICOS](#)

Ensemble Data Assimilation [\[go to top\]](#)

1. Introduction

Data assimilation is the name of a process by which observations of the 'state' of a system help to constrain the behavior of the system in time. An example of one of the earliest applications of data assimilation is the system in which the trajectory of a flying rocket is constantly (and rapidly) adjusted based on information of its current position to guide it to its exact final destination. Another example of data assimilation is a weather model that gets updated every few hours with measurements of temperature and other variables, to improve the accuracy of its forecast for the next day, and the next, and the next. Data assimilation is usually a cyclical process, as estimates get refined over time as more observations about the "truth" become available. Mathematically, data assimilation can be done with any number of techniques. For large systems, so-called variational and ensemble techniques have gained most popularity. Because of the size and complexity of the systems studied in most fields, data assimilation projects inevitably include supercomputers that model the known physics of a system. Success in guiding these models in time often depends strongly on the number of observations available to inform on the true system state.

In CarbonTracker, the model that describes the system contains relatively simple descriptions of biospheric and oceanic CO₂ exchange, as well as fossil fuel and fire emissions. In time, we alter the behavior of this model by adjusting a set of parameters as described in the next section.

2. Detailed Description

The four surface flux modules drive instantaneous CO₂ fluxes in CarbonTracker according to:

$$F(x, y, t) = \lambda(x, y, t) \cdot F_{\text{Bio}}(x, y, t) + \lambda(x, y, t) \cdot F_{\text{Occ}}(x, y, t) + F_{\text{ff}}(x, y, t) + F_{\text{fire}}(x, y, t)$$

Where λ represents a set of linear scaling factors applied to the fluxes, to be estimated in the assimilation. These scaling factors are the final product of our assimilation and together with the modules determine the fluxes we present in CarbonTracker. Note that no scaling factors are applied to the fossil fuel and fire modules.

2.1 Land-surface classification

The scaling factors λ are estimated for each week and assumed constant over this period. Each scaling factor is associated with a particular gridbox of the global domain. We chose an approach in which the ocean grid boxes are combined into 30 large basins encompassing large-scale ocean circulation features, as in the TransCom inversion study (e.g. Gurney et al., [2002]). The terrestrial biosphere grid boxes are combined up according to ecosystem type as well as geographical location. Thereto, each of the 11 TransCom land regions contains a maximum of 19 ecosystem types summarized in the table below for Europe.

Ecosystem types considered on 1x1 degree for the terrestrial flux inversions is based on [Olson, \[1992\]](#). Note that we have adjusted the original 29 categories into only 19 regions. This was done mainly to fill the unused categories 16,17, and 18, and to group the similar (from our perspective) categories 23–26+29. The table below shows each vegetation category considered. Percentages indicate the area associated with each category for Europe rounded to one decimal.

Ecosystem Types and area in Europe		
category	Olson V 1.3a	%
1	Conifer Forest	14.0
2	Broadleaf Forest	2.5
3	Mixed Forest	8.9
4	Grass/Shrub	8.0
5	Tropical Forest	0.1
6	Scrub/Woods	2.8
7	Semitundra	4.9
8	Fields/Woods/Savanna	6.6
9	Northern Taiga	2.2
10	Forest/Field	11.5
11	Wetland	0.7
12	Deserts	0.1
13	Shrub/Tree/Suc	0.0
14	Crops	22.3
15	Conifer Snowy/Coastal	0.0
16	Wooded tundra	1.6
17	Mangrove	0.0
18	Ice and Polar desert	0.0
19	Water	13.8
99	All	100.0

Each 1x1 degree pixel of our domain was assigned one of the categories above bases on the Olson category that was most prevalent in the 0.5x0.5 degree underlying area.

2.2 Ensemble Size and Localization

The ensemble system used to solve for the scalar multiplication factors is similar to that in Peters et al. [2005] and based on the square root ensemble Kalman filter of Whitaker and Hamill, [2002]. We have restricted the length of the smoother window to only five weeks as we found the derived flux patterns within Europe and North America to be robustly resolved well within that time. We caution the CarbonTracker users that although the North American and European flux results were found to be robust after five weeks, regions of the world with less dense observational coverage (the tropics, Southern Hemisphere, and parts of Asia) are likely to be poorly observable even after more than a month of transport and therefore less robustly resolved. Although longer assimilation windows, or long prior covariance length-scales, could potentially help to constrain larger scale emission totals from such areas, we focus our analysis here on a region more directly constrained by real atmospheric observations.

Ensemble statistics are created from 150 ensemble members, each with its own background CO₂ concentration field to represent the time history (and thus covariances) of the filter. In contrast to our earlier system design, we currently do not apply any localization to the statevector.

2.3 Dynamical Model

In CarbonTracker, the dynamical model is applied to the mean parameter values λ as:

$$\lambda_t^b = (\lambda_{t-2}^a + \lambda_{t-1}^a + \lambda^p) / 3.0$$

Where "a" refers to analyzed quantities from previous steps, "b" refers to the background values for the new step, and "p" refers to real *a-priori* determined values that are fixed in time and chosen as part of the inversion set-up. Physically, this model describes that parameter values λ for a new time step are chosen as a combination between optimized values from the two previous time steps, and a fixed prior value. This operation is similar to the simple persistence forecast used in Peters et al. [2005], but represents a smoothing over three time steps thus dampening variations in the forecast of λ^b in time. The inclusion of the prior term λ^p acts as a regularization [Baker et al., 2006] and ensures that the parameters in our system will eventually revert back to predetermined prior values when there is no information coming from the observations. Note that our dynamical model equation does not include an error term on the dynamical model, for the simple reason that we don't know the error of this model. This is reflected in the treatment of covariance, which is always set to a prior covariance structure and not forecast with our dynamical model.

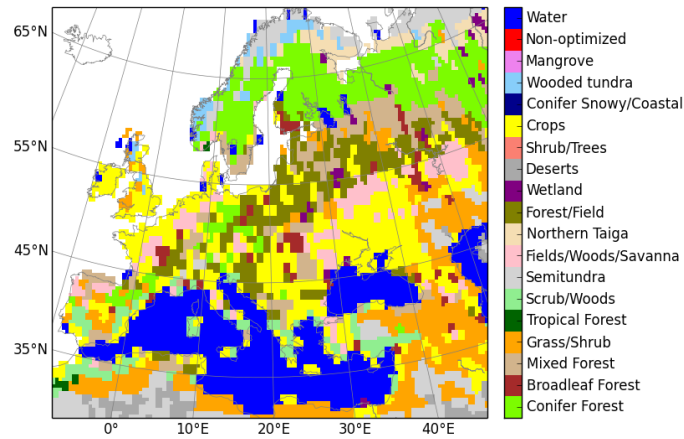
2.4 Covariance Structure

Prior values for λ^p are all 1.0 to yield fluxes that are unchanged from their values predicted in our modules. The prior covariance structure P^p describes the magnitude of the uncertainty on each parameter, plus their correlation in space.

In each of these regions on the northern hemisphere, individual $\lambda(x,y)$ parameters are coupled through an isentropic covariance structure which makes two boxes i and j at a distance d of each other have a covariance C of

$$C = 0.64 \cdot \exp(-d/L).$$

In this formula the covariance length scale L varies across the globe. Over Boreal and Temperate North America where the observation network is relatively dense, $L=300$ km, but in Boreal and Temperate Asia the number of observations constrains a much smaller number of parameters individually and we chose $L=1000$ km. In Europe, with its strongly heterogeneous land-use and land management and large volume of observations available we took $L=200$ km. In the rest of the world, the length scale is taken infinitely large, coupling fully all grid boxes and associated λ 's in the tropics and southern hemisphere.



The figure shows ecoregions for Europe ([click here for global land ecoregions](#)). Note that there is currently no requirement for ecoregions to be contiguous, and a single scaling factor can be applied to the same vegetation type on both sides of a continent.

Theoretically, this approach leads to a total number of 9835 optimizable scaling factors λ each week, but the actual number is smaller since not every ecosystem type is represented in each **TransCom region**, and because we decided not to optimize parameters for ice-covered regions, inland water bodies, and desert. The total flux coming out of these last regions is negligibly small. It is important to note that even though many parameters are available to scale the fluxes, the imposed covariance structure reduces the number of degrees of freedom to about 1100 each week.

Furthermore, all ecosystems *within* tropical **TransCom regions** are coupled decreasing exponentially with distance since we do not believe the current observing network can constrain tropical fluxes on sub-continental scales, and want to prevent large dipoles to occur in the tropics.

In our standard assimilation, the chosen standard deviation is 80% on land parameters, and 40% on ocean parameters. This reflects more prior confidence in the ocean fluxes than in terrestrial fluxes, as is assumed often in inversion studies and partly reflects the lower variability and larger homogeneity of the ocean fluxes. All parameters have the same variance within the land or ocean domain. Because the parameters multiply the net-flux though, ecosystems with larger weekly mean net fluxes have a larger variance in absolute flux magnitude.

3. Further Reading

- [Whitaker and Hamill, 2002 paper](#)
- [Peters et al., 2005 paper](#)
- [Olson ecosystem types, data](#)